First-principles multielectron calculations of Ni $L_{2,3}$ NEXAFS and ELNES for $LiNiO_2$ and related compounds

Hidekazu Ikeno and Isao Tanaka
Department of Materials Science and Engineering, Kyoto University, Yoshida, Sakyo, Kyoto 606-8501, Japan

Yukinori Koyama
Department of Materials Science and Engineering, Nagoya University, Furo, Chikusa, Nagoya 464-8603, Japan

Teruyasu Mizoguchi
Institute of Engineering Innovation, The University of Tokyo, Yayoi, Bunkyo, Tokyo 113-8656, Japan

Kazuyoshi Ogasawara
School of Science and Technology, Kwansei Gakuin University, Sanda, Hyogo 669-1337, Japan
(Received 15 March 2005; revised manuscript received 24 June 2005; published 17 August 2005)

A technique to compute 3*d* transition-metal $L_{2,3}$-edge near-edge x-ray-absorption fine structure (NEXAFS) and electron energy-loss near-edge structure (ELNES) is adopted to predict and interpret spectra from NiO, $LiNiO_2$, and NiO_2. Multielectron wave functions were obtained as a linear combination of Slater determinants. The Slater determinants were constructed using all Ni-2*p*- and Ni-3*d*-based molecular orbitals, instead of atomic orbitals, obtained by solving the Dirac equation within the local density approximation for NiO_6^{m-} clusters ($m=10$, 9, and 8). The O-2*p* contributions through covalency can therefore be included automatically without any other scheme. Experimental ELNES for the three compounds were satisfactory reproduced by the present calculations, which unambiguously shows that Ni atoms are Ni(III) with a low-spin state in $LiNiO_2$, and Ni(IV) with a low-spin state in NiO_2. The origin of satellite peaks in the spectra is also clarified. The present method is based on the robust multielectron quantum theory, which could be applied to the analysis and prediction of $L_{2,3}$-edge spectra of other transition-metal compounds.

DOI: 10.1103/PhysRevB.72.075123 PACS number(s): 78.70.Dm, 78.20.Bh, 71.15.Rf

I. INTRODUCTION

Both near-edge x-ray-absorption fine structure (NEXAFS) and electron energy-loss near-edge structure (ELNES) are powerful techniques to observe electronic structures of selected elements. When measured using transmission electron microscopy, ELNES is identical to NEXAFS. We will hereafter refer only to NEXAFS. However, the same discussion can be made for ELNES. $L_{2,3}$ NEXAFS of a 3*d* transition-metal element mainly corresponds to electric dipole transition from its 2*p* core levels to 3*d* orbitals. Minor contributions because of electric dipole transitions from 2*p* to *ns* ($n=4,5,\ldots$) and the electric quadrupole transition are negligible. Hence, the spectra directly reflect electronic structure of the 3*d* orbitals of the selected element. In spite of its potential usefulness, the $L_{2,3}$-edge is less used than the *K*-edge. One of the reasons is the difficulty of interpreting the measured spectra.

It has been demonstrated that most of *K* NEXAFS can be reproduced by a standard first-principles method within the one-electron approximation if the effect of a core hole is properly taken into account.[1–6] On the other hand, the $L_{2,3}$ NEXAFS of 3*d* transition-metal compounds cannot be reproduced using such methods. It is sometimes misunderstood that the $L_{2,3}$ NEXAFS of 3*d* transition-metal compounds can be obtained simply by overlaying the spectrum by the one-electron calculations with proper L_3-L_2 splitting and L_3/L_2 intensity ratio. However, strong correlation among spatially localized 3*d* electrons and that between the core-hole and the excited electron entirely changes the spectral shape. The 3*d* electrons show widely spread multiplet structures even without a 2*p* core hole because of the strong correlation. The presence of the 2*p* core hole introduces further complexity into the spectra. Therefore, one-electron calculations are useless for $L_{2,3}$ NEXAFS, in general. Recently, theoretical methods to explicitly include correlation between the core hole and the excited electron have been reported.[7,8] However, none of them computed the multiplet structures because of the strong correlation among 3*d* electrons.

Multiplet structures of isolated atoms were well studied both by experiment and theory. Crystal field effects have been incorporated into an atomic multiplet program using group theoretical formalism, which is called the crystal-field atomic multiplet program.[9,10] Although this approach has been successful in reproducing multiplet structures of many transition-metal compounds, it employs a number of adjustable parameters and therefore cannot be used to predict multiplet structures *a priori*. Another problem of this approach resides in the treatment of ligand orbitals. Contribution of ligand orbitals as a result of covalent bonding can only be indirectly included in the crystal-field theory. Establishment of a first-principles method beyond the one-electron approximation that takes into account the multielectron interactions is, therefore, highly desirable. In order to treat the electronic

transition from a core orbital, relativistic effects should also be considered. One part of the relativistic effects is known as spin-orbit coupling. It can be automatically included by solving Dirac equation instead of Schrödinger equation.

By this group of the authors, a different calculation technique, which can deal directly with both the multielectron problem and the relativistic effect, has been developed.[11] Electronic correlations among $3d$ electrons and a $2p$ core hole were rigorously accounted for by taking multiple Slater determinants composed of molecular orbitals. The technique can be used to predict $L_{2,3}$-edge spectra quantitatively without any adjustable parameters. In the present work, the method is applied to the Ni $L_{2,3}$ NEXAFS of three kinds of nickel oxides, i.e., NiO, $LiNiO_2$, and NiO_2 (Li-extracted $LiNiO_2$). Then we show a method to investigate the origin of satellite peaks in the spectra in terms of symmetry and electronic configurations. $LiNiO_2$ and NiO_2 are both important in lithium-ion batteries as cathode materials. Changes in the electronic structure due to lithium extraction (such as valency and spin-state of nickel ions) are therefore very interesting, not only from a fundamental viewpoint, but also for development of new materials. Ni $L_{2,3}$ NEXAFS should be an ideal tool to investigate them since it provides direct information of the Ni-$3d$ states.

II. COMPUTATIONAL PROCEDURE

The crystal structures of the three compounds are known by experiments.[12,13] Ni ions are coordinated by six O ions. The model clusters of NiO_6^{m-}, which are composed of a Ni ion and six nearest-neighbor O ions, were used. The total number of electrons in the cluster was obtained from formal charges, thus $m=10$, 9, and 8 for NiO [Ni(II)], $LiNiO_2$ [Ni(III)], and NiO_2 [Ni(IV)], respectively. The cluster model of NiO shows O_h symmetry, while those of $LiNiO_2$ and NiO_2 show D_{3d} symmetry. The Ni-O bond lengths were 0.2090, 0.1967, and 0.1861 nm in NiO, $LiNiO_2$, and NiO_2, respectively. In order to take account of effective Madelung potential, an array of point charges was set at the external atomic sites in the calculations.

The computational procedure of multielectron calculations that we are going to explain is equivalent to the "configuration interaction" calculations that are popular in quantum chemistry. However, in order to avoid misunderstanding and confusion, we do not use the words "configuration interaction" because these words sometimes have different meanings between quantum chemistry and atomic physics. Before presenting a detailed description of our procedures, let us explain our terminology.

We use density-functional calculations to obtain molecular orbitals (MO). Atomic orbitals (AO) are used as basis functions for the MO calculations. Slater determinants are constructed using these MO as components. Multielectron eigenstates can be computed by diagonalizing the multielectron Hamiltonian to be given in Eq. (1). Multielectron wave functions are formed by a linear combination of Slater determinants, which will be given in Eq. (3). When we use the term "state," such as in initial state and final state, it corresponds to individual multielectron eigenstates. In quantum chemistry, the term "configuration" corresponds to each of the Slater determinants. In atomic physics, on the other hand, the term "configuration" corresponds to a set of Slater determinants that have the same number of electrons in the atomic orbitals, such as $(2p)^5(3d)^3$ and $(2p)^6(3d)^2$. We adopt the latter way to define configuration.

In the present study, fully relativistic MO calculations were carried out by solving Dirac equations with the local density approximation (LDA) using the code that was originally described in Ref. 14. Recently the code has been modified and successful in calculations of optical spectra of many laser crystals.[15,16] In this code, four-component relativistic molecular orbitals are expressed as linear combination of AO (LCAO). The numerically generated four-component relativistic AO ($1s$ to $4p$ for Ni and $1s$ to $2p$ for O) were used as basis functions for MO. After one-electron calculations of relativistic MO, we made multielectron calculations.

Only Ni $2p$ orbitals and MO mainly composed of Ni $3d$ orbitals (as will be described by ϕ_{3d}, or by t_{2g} and e_g) were considered explicitly for the multielectron calculation, since inclusion of all N electrons in the cluster requires a prohibitive amount of computational time and resources. An effective multielectron Hamiltonian is expressed as

$$H = \sum_{i=1}^{n} h(\boldsymbol{r}_i) + \sum_{i=1}^{n} \sum_{j>i}^{n} \frac{1}{|\boldsymbol{r}_i - \boldsymbol{r}_j|}, \tag{1}$$

where n is the number of electrons in the selected MO. The one-electron operator $h(\boldsymbol{r}_i)$ is given by

$$h(\boldsymbol{r}_i) = c\tilde{\boldsymbol{\alpha}}\boldsymbol{p}_i + c^2\tilde{\beta} - \sum_{\nu} \frac{Z_\nu}{|\boldsymbol{r}_i - \boldsymbol{R}_\nu|} + V'(\boldsymbol{r}_i), \tag{2}$$

where $\tilde{\boldsymbol{\alpha}}, \tilde{\beta}$ are Dirac matrices, c is the velocity of light, $\boldsymbol{p}_i$ is the momentum operator, Z_ν is the charge of νth nucleus, and $V'(\boldsymbol{r}_i)$ is the potential from the other $(N-n)$ electrons. In this approach, the Coulomb interaction and exchange-correlation interaction among the selected n electrons are considered explicitly, whereas those interactions between the selected n electrons and the remaining $(N-n)$ electrons are expressed as an effective potential of $V'(\boldsymbol{r}_i)$. The explicit form of $V'(\boldsymbol{r}_i)$ as derived by Watanabe and Kamimura[17] was adopted.

As basis functions to diagonalize the multielectron Hamiltonians shown in Eq. (1), all possible Slater determinants for given configurations that are related to Ni $L_{2,3}$ NEXAFS were used. The multielectron wave functions were then expressed as a linear combination of those Slater determinants,

$$\Psi_i = \sum_{i=1}^{M} C_{ip}\Phi_p, \tag{3}$$

where Ψ_i is the ith multielectron wave function, Φ_p is the pth Slater determinant, and C_{ip} is the coefficient. Ni $L_{2,3}$ NEXAFS of NiO is due to the transitions from $(2p)^6(\phi_{3d})^8$ to $(2p)^5(\phi_{3d})^9$, where ϕ_{3d} denotes the MO mainly composed of Ni $3d$ orbitals. The number of possible Slater determinants for $(2p)^6(\phi_{3d})^8$ is 45 $(={}_6C_6 \times {}_{10}C_8)$ and that for $(2p)^5(\phi_{3d})^9$ is 60 $(={}_6C_5 \times {}_{10}C_9)$. Thus 105 Slater determinants were used as bases for multielectron wave functions. For $LiNiO_2$

[Ni(III)], Ni $L_{2,3}$ NEXAFS corresponds to the transitions from $(2p)^6(\phi_{3d})^7$ to $(2p)^5(\phi_{3d})^8$. The number of Slater determinants for $(2p)^6(\phi_{3d})^7$ is 120 $(={}_6C_6\times{}_{10}C_7)$ and that for $(2p)^5(\phi_{3d})^8$ is 270 $(={}_6C_5\times{}_{10}C_8)$. Therefore, there were 390 Slater determinants used. In the case of NiO_2 [Ni(VI)], Ni $L_{2,3}$ NEXAFS corresponds to the transitions from $(2p)^6(\phi_{3d})^6$ to $(2p)^5(\phi_{3d})^7$. The number of determinants is 210 $(={}_6C_6\times{}_{10}C_6)$ for $(2p)^6(\phi_{3d})^6$ and 720 $(={}_6C_5\times{}_{10}C_7)$ for $(2p)^5(\phi_{3d})^7$, thus, 930 in total.

The oscillator strength of the electric dipole transition averaged over all directions is given by

$$I_{if}=\frac{2}{3}(E_f-E_i)\left|\left\langle\Psi_i\left|\sum_{k=1}^{n}\boldsymbol{r}_k\right|\Psi_f\right\rangle\right|^2 \quad (4)$$

where Ψ_i and Ψ_f are multielectron wave functions for the initial state and the final state, while E_i and E_f are their energies. This procedure was pointed out to overestimate the absolute transition energy typically by $<1\%$.[11] In Ref. 11, the transition energy was corrected by taking the orbital-energy difference between single-electron orbitals for the Slater's transition state as a reference. We have adopted the same procedure in the present study.

III. RESULTS AND DISCUSSION

A. Initial states

First, we made relativistic molecular-orbital calculations within LDA. The MO obtained by LDA calculations were used as components of Slater determinants in the multielectron calculations. It is generally accepted that the magnitude of covalent bonding between the 3*d* orbital of the transition element and 2*p* orbital of oxygen increases with the increase of the formal charge of the transition element. In order to quantify the trend, Mulliken's population analysis[18] has been made. We found that the atomic-orbital population of O-2*p* is 3.3%, 7.2%, and 17.6% in t_{2g} for NiO, $LiNiO_2$, and NiO_2, respectively. The population is greater in e_g than in t_{2g}, i.e., 14.3%, 30.3%, and 34.8% for NiO, $LiNiO_2$ and NiO_2, respectively. The substantial mixing of O-2*p* in these compounds clearly implies the superiority of using MO instead of AO as components of Slater determinants. Contribution of covalency can be thereby included automatically without implementation of any other scheme. It should be noted that the expressions t_{2g} and e_g are not rigorously right within the relativistic theory (see Fig. 1). Instead, the representations of the double group, such as $e_{5/2g}$ and $g_{3/2g}$, should be employed. They are equivalent to γ_{7g} (γ_7^+) and γ_{8g} (γ_8^+) using the Bethe symbol.[19] Furthermore, t_{2g} and e_g orbitals split because of the trigonal distortion of the crystal field, since the point group symmetry of the cluster models for $LiNiO_2$ and NiO_2 is reduced to D_{3d} symmetry from O_h symmetry. However, the energy splitting in t_{2g} and e_g orbitals because of relativistic effects and trigonal distortion is one-tenth the order of the energy splitting between t_{2g} and e_g, i.e., $10Dq$. Therefore, the expressions t_{2g} and e_g will be adopted in the following part of this paper for simplicity.

Using the relativistic MO, multielectron calculations were carried out. First, we show the result for the initial states.

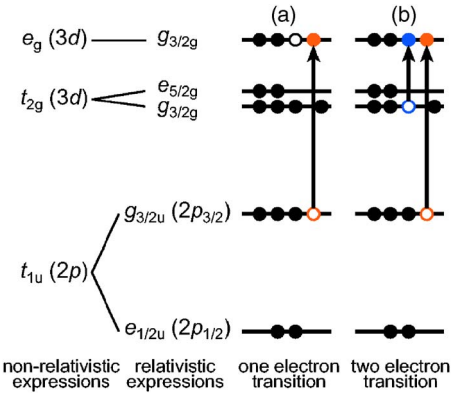

FIG. 1. (Color online) Schematic one-electron view of eigenvalues of NiO_6^{10-} in O_h symmetry and two ways for the electronic transition from $2p_{3/2}(g_{3/2u})$ to $e_g(g_{3/2g})$.

Considering the orthonormality of the Slater determinants, the composition of the *p*th Slater determinant in the *i*th eigenstate is simply given by $|C_{ip}|^2$. The contributions from several configurations are listed in Table I. In the one-electron scheme, the initial configuration of NiO can be described as 100% $(2p_{1/2})^2(2p_{3/2})^4(t_{2g})^6(e_g)^2$. The result of multielectron calculation shows that the $(2p_{1/2})^2(2p_{3/2})^4(t_{2g})^6(e_g)^2$ contribution is 96.7% for the initial

TABLE I. Compositions of configurations in the multielectron wave functions that correspond to the initial state of Ni $L_{2,3}$ NEXAFS

	Configurations	(%)
NiO	$(2p_{1/2})^2(2p_{3/2})^4(t_{2g})^6(e_g)^2$	96.7
	$(2p_{1/2})^2(2p_{3/2})^4(t_{2g})^5(e_g)^3$	1.8
	$(2p_{1/2})^2(2p_{3/2})^4(t_{2g})^4(e_g)^4$	1.5
$LiNiO_2$ low-spin	$(2p_{1/2})^2(2p_{3/2})^4(t_{2g})^6(e_g)^1$	98.1
	$(2p_{1/2})^2(2p_{3/2})^4(t_{2g})^5(e_g)^2$	0.4
	$(2p_{1/2})^2(2p_{3/2})^4(t_{2g})^4(e_g)^3$	1.5
$LiNiO_2$ high-spin	$(2p_{1/2})^2(2p_{3/2})^4(t_{2g})^6(e_g)^1$	0.2
	$(2p_{1/2})^2(2p_{3/2})^4(t_{2g})^5(e_g)^2$	96.6
	$(2p_{1/2})^2(2p_{3/2})^4(t_{2g})^4(e_g)^3$	3.2
NiO_2 low-spin	$(2p_{1/2})^2(2p_{3/2})^4(t_{2g})^6(e_g)^0$	96.7
	$(2p_{1/2})^2(2p_{3/2})^4(t_{2g})^5(e_g)^1$	1.8
	$(2p_{1/2})^2(2p_{3/2})^4(t_{2g})^4(e_g)^2$	1.5
	$(2p_{1/2})^2(2p_{3/2})^4(t_{2g})^3(e_g)^3$	0.0
NiO_2 middle-spin	$(2p_{1/2})^2(2p_{3/2})^4(t_{2g})^6(e_g)^0$	0.0
	$(2p_{1/2})^2(2p_{3/2})^4(t_{2g})^5(e_g)^1$	97.4
	$(2p_{1/2})^2(2p_{3/2})^4(t_{2g})^4(e_g)^2$	2.2
	$(2p_{1/2})^2(2p_{3/2})^4(t_{2g})^3(e_g)^3$	0.4
NiO_2 high-spin	$(2p_{1/2})^2(2p_{3/2})^4(t_{2g})^6(e_g)^0$	0.0
	$(2p_{1/2})^2(2p_{3/2})^4(t_{2g})^5(e_g)^1$	0.1
	$(2p_{1/2})^2(2p_{3/2})^4(t_{2g})^4(e_g)^2$	99.6
	$(2p_{1/2})^2(2p_{3/2})^4(t_{2g})^3(e_g)^3$	0.3

TABLE II. Number of possible transitions and their irreducible representations for four different types of transitions in Ni $L_{2,3}$-edge NEXAFS of NiO_6^{10-} with O_h symmetry.

Core hole	Excited electron	Number of eigenstates	Number of dipole allowed eigenstates	
$g_{3/2u}$ $(2p_{3/2})$	$g_{3/2g}$ $(t_{2g}+e_g)$	32	16	$A_{1u}+A_{2u}+E_u+2T_{1u}+2T_{2u}$
$g_{3/2u}$ $(2p_{3/2})$	$e_{5/2g}$ (t_{2g})	8	0	$E_u+T_{1u}+T_{2u}$
$e_{1/2u}$ $(2p_{1/2})$	$g_{3/2g}$ $(t_{2g}+e_g)$	16	8	$E_u+T_{1u}+T_{2u}$
$e_{1/2u}$ $(2p_{1/2})$	$e_{5/2g}$ (t_{2g})	4	0	$A_{2u}+T_{2u}$

state of NiO. Although we will take account of all configurations for the NEXAFS calculations to describe the initial state, the $(2p_{1/2})^2(2p_{3/2})^4(t_{2g})^6(e_g)^2$ configuration is found to be predominant, which agrees well with our intuition. Similar multielectron calculations were made for $LiNiO_2$ and NiO_2 imposing several spin configurations. It should be noted that more than 95% of the initial states in all cases are composed of the dominant configuration.

B. Multielectron eigenstates and theoretical NEXAFS

1. NiO

Figure 1 schematically shows a one-electron view of eigenvalues of the NiO_6^{10-}cluster and the electronic transition from $2p_{3/2}$ to e_g ($g_{3/2g}$ in the relativistic expression). Since the t_{2g} orbitals also include $g_{3/2g}$ representation when translated into the relativistic expression, two kinds of transitions as shown in Fig. 1 need to be considered for L_3 NEXAFS. Their final configurations are $(2p_{1/2})^2(2p_{3/2})^3(t_{2g})^6(e_g)^3$ and $(2p_{1/2})^2(2p_{3/2})^3(t_{2g})^5(e_g)^4$, respectively. A number of different ways to put a hole in the $2p_{3/2}$ and seven electrons to the $g_{3/2g}$ orbitals is ${}_4C_1 \times {}_8C_7=32$, which include both of the two final configurations. Only the transition to $(2p_{1/2})^2(2p_{3/2})^3(t_{2g})^6(e_g)^3$ is allowed as an electric dipole transition. The allowed 16 transitions can be classified as $A_{1u}+A_{2u}+E_u+2T_{1u}+2T_{2u}$ under O_h point group symmetry. The number of transitions and their irreducible representations for the four different types of transitions are summarized in Table II.

Figure 2(a) shows all 60 of the multielectron eigenvalues of the final states using vertical bars. They are classified by colors according to their final configurations. For example, red bars correspond to final configurations of $(2p_{1/2})^2(2p_{3/2})^3(t_{2g})^6(e_g)^2$. Figure 2(b) shows computed oscillator strength of the electric-dipole transition to each eigenstate with black bars. As explained in Table I, the initial states are predominantly composed of $(2p_{1/2})^2(2p_{3/2})^4(t_{2g})^6(e_g)^2$. Therefore, the transitions to final configurations $(2p_{1/2})^2(2p_{3/2})^3(t_{2g})^6(e_g)^3$ [red bars in Fig. 2(a)] and $(2p_{1/2})^1(2p_{3/2})^4(t_{2g})^6(e_g)^3$ [magenta bars in Fig. 2(a)] dominate to the oscillator strengths of Ni $L_{2,3}$ NEXAFS because of the electric dipole selection rule. Figure 2(c) summarizes compositions of those two kinds of final configurations, i.e., $(2p_{1/2})^2(2p_{3/2})^3(t_{2g})^6(e_g)^3$ [red bars in Fig. 2(a)] and $(2p_{1/2})^1(2p_{3/2})^4(t_{2g})^6(e_g)^3$ [magenta bars in Fig. 2(a)]. Theoretical spectrum of the Ni $L_{2,3}$ NEXAFS as shown in top panels was made by broadening the oscillator strengths using Gaussian functions with the dispersion $\sigma=0.4$ eV [or full width at half maximum (FWHM)=0.94 eV]. The oscillator strengths are superposed on the theoretical spectrum with shortened black bars.

Using these diagrams, one can clearly interpret the origin of peaks in the theoretical spectrum. Peak *a* is composed of eigenstates that can be classified into A_{2u}, E_u, T_{1u}, and T_{2u}. Peak *b* can be ascribed predominantly to T_{1u}. This shows higher transition energy of peak *b* than peak *a*, because the eigenstate corresponding to peak *b* is a mixture of two configurations as shown in Fig. 1. As can be seen in Fig. 2(a), 24% of the contribution is due to the $(2p_{1/2})^2(2p_{3/2})^3(t_{2g})^5(e_g)^4$ [green bars in Fig. 2(a)]. This configuration corresponds to the two electrons excitation shown in Fig. 1(b) and it is not allowed as an electric dipole transition. Although the component does not contribute to the oscillator strength, the mixing of the $t_{2g} \rightarrow e_g$ excitation with the $2p_{3/2} \rightarrow e_g$ excitation makes the transition energy higher than that without such mixing. The small peak *c* can be ascribed to T_{2u}, which is energetically much more expensive because the major contribution to this eigenstate is the two electrons excitation. The origin of peaks *d* to *f* can be interpreted in a similar manner.

2. $LiNiO_2$

In the case of $LiNiO_2$, the initial configuration is $(2p)^6(\phi_{3d})^7$. Two different spin configurations can be candidates for the initial configuration. One is low-spin configuration, which is mainly composed of $(2p_{1/2})^2(2p_{3/2})^4(t_{2g})^6(e_g)^1$ and the other is high-spin configuration, which is mainly composed of $(2p_{1/2})^2(2p_{3/2})^4(t_{2g})^5(e_g)^2$, as can be seen in Table I. Multielectron calculations were carried out, and 270 final states for Ni $L_{2,3}$ NEXAFS were obtained as shown in Fig. 3(a). They are distinguished by colors according to their final configurations. Since the NiO_6^{9-} cluster in $LiNiO_2$ shows D_{3d} symmetry, two irreducible representations, $E_{1/2u}$ and $E_{3/2u}$, appear in the final states. Depending on the choice of the initial configuration, the dipole transition probability is quite differ-

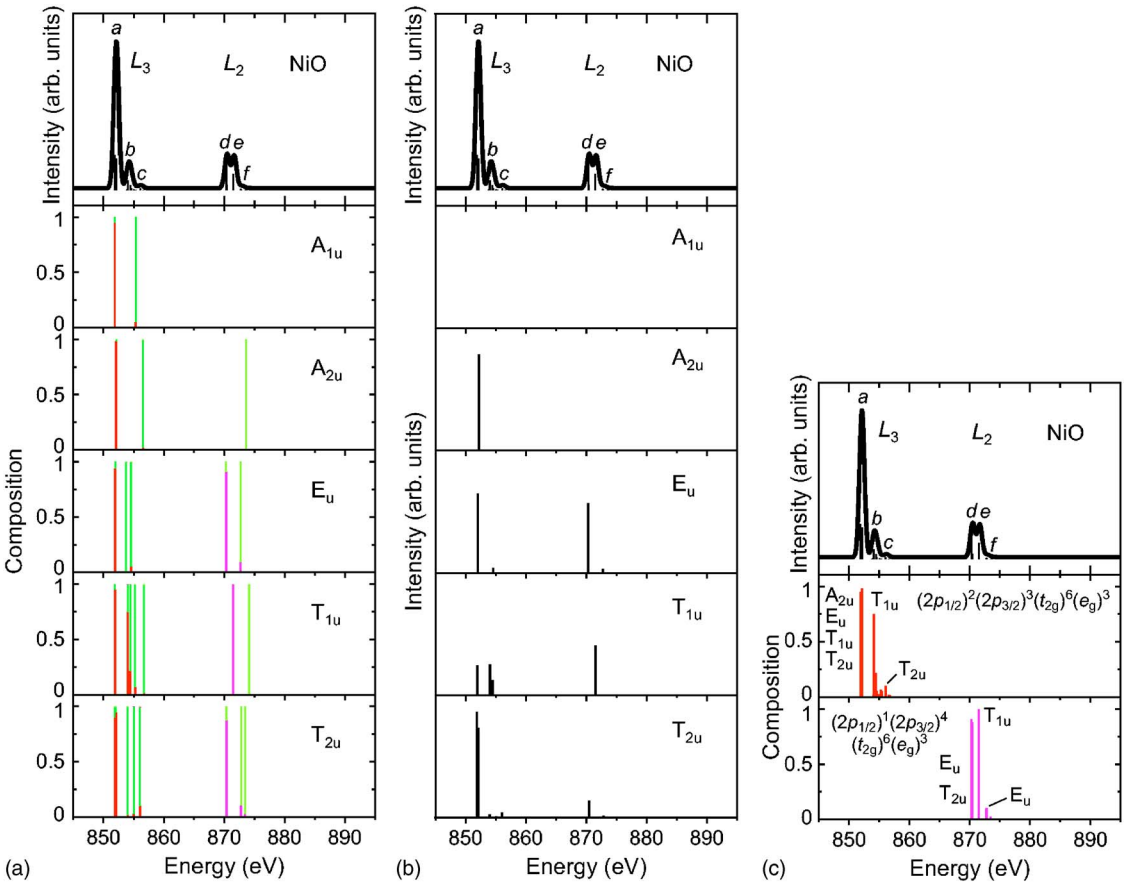

FIG. 2. (Color online) (a) Theoretical $L_{2,3}$-edge NEXAFS and ELNES for Ni(II) in NiO is shown in upper panel. Bars in upper panel shows the oscillator strengths for multielectron eigenstates. The following panels show the composition of final configurations for multielectron eigenstates in five symmetries. They are classified according to final configurations as distinguished by colors: red $(2p_{1/2})^2(2p_{3/2})^3(t_{2g})^6(e_g)^3$, green $(2p_{1/2})^2(2p_{3/2})^3(t_{2g})^5(e_g)^4$, magenta $(2p_{1/2})^1(2p_{3/2})^4(t_{2g})^6(e_g)^3$, and yellowish green $(2p_{1/2})^1(2p_{3/2})^4(t_{2g})^5(e_g)^4$. (b) Oscillator strengths for all final states in five symmetries. The lengths of bars were multiplied by 3 from that of the oscillator strengths superimposed on the theoretical spectrum (top panel) for easy visualization. (c) Compositions of final configurations for the dipole allowed transitions, i.e., $(2p_{1/2})^2(2p_{3/2})^3(t_{2g})^6(e_g)^3$ (red bars in a) and $(2p_{1/2})^1(2p_{3/2})^4(t_{2g})^6(e_g)^3$ (magenta bars in a).

ent. When the initial configuration is low spin, i.e., $(2p)^6(t_{2g})^6(e_g)^1$ configuration, only the transition to $(2p)^5(t_{2g})^6(e_g)^2$ is allowed. On the other hand, when the initial configuration is high spin, i.e., $(2p_{1/2})^2(2p_{3/2})^4(t_{2g})^5(e_g)^2$ configuration, transition can be allowed to either $(2p)^5(t_{2g})^6(e_g)^2$ or $(2p)^5(t_{2g})^5(e_g)^3$. The contributions from four final configurations are shown in Fig. 3(b). Theoretical spectrum of the Ni $L_{2,3}$ NEXAFS was made in the same way as in Fig. 2 with dispersion of $\sigma=0.4$ eV. As can be found from these figures, peaks $a-c$ of the low-spin spectrum can be ascribed to the eigenstates that are predominantly composed of $(2p_{1/2})^2(2p_{3/2})^3(t_{2g})^6(e_g)^2$ [red bars in Fig. 3(a)]. Hence, peaks $a-c$ can be translated as the $2p_{3/2}\rightarrow e_g$ excitation. Eigenstates that are responsible for the tiny peaks, d and e, at higher energies are predominantly composed of $(2p_{1/2})^2(2p_{3/2})^3(t_{2g})^5(e_g)^3$ [green bars in Fig. 3(a)], which is dipole forbidden. They are located much higher in transition energy than peaks $a-c$ because of the mixture of the $t_{2g}\rightarrow e_g$ and $2p_{3/2}\rightarrow e_g$ excitations. A similar analysis can be applied to L_2-edge. Peaks $f-h$ are mainly due to the transition to $(2p_{1/2})^1(2p_{3/2})^4(t_{2g})^6(e_g)^2$ [magenta bars in Fig. 3(a)]. Peaks i and j are higher in energy because their major component is a dipole-forbidden two-electron excitation of $2p_{1/2}\rightarrow e_g$ with the $t_{2g}\rightarrow e_g$ excitation.

When the initial configuration is high-spin, both of L_3 and L_2 peaks of the theoretical NEXAFS of NiO_6^{9-} can be categorized into two groups originating from two different configurations. In the L_3-edge, peak a' can be ascribed to $2p_{3/2}\rightarrow t_{2g}$ transition, and peaks $b'-d'$ to $2p_{3/2}\rightarrow e_g$ transition. Likewise in the L_2-edge, peaks e' and f' can be ascribed to $2p_{1/2}\rightarrow t_{2g}$ transition, and peaks g' and h' to $2p_{1/2}\rightarrow e_g$ transition.

3. NiO_2

Results for NiO_2 using a NiO_6^{8-} cluster with D_{3d} symmetry are summarized in Fig. 4. Within the one-electron scheme, only two different spin configurations, i.e., high- and low-spin, are possible since the initial configuration is $(2p)^6(\phi_{3d})^6$. On the other hand within the multielectron scheme, some other spin configurations can be taken as initial configurations. An example is a the middle-spin configuration, which is mainly composed of $(2p_{1/2})^2(2p_{3/2})^4(t_{2g})^5(e_g)^1$ configuration. Eigenvalues for the 720 final states for Ni $L_{2,3}$ NEXAFS in the three irreducible

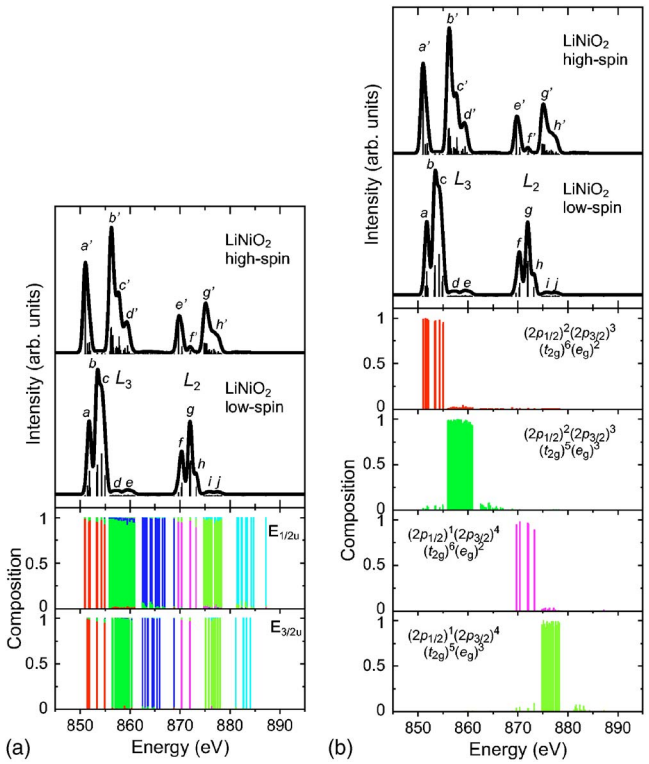

FIG. 3. (Color online) (a) Theoretical $L_{2,3}$-edge NEXAFS and ELNES for a low and high-spin states for Ni(III) in $LiNiO_2$ are shown in the upper two panels. The following panels show the composition of final configurations for multielectron eigenstates in $E_{1/2u}$ and $E_{3/2u}$ symmetries. They are classified according to final configurations as distinguished by colors: red $(2p_{1/2})^2(2p_{3/2})^3(t_{2g})^6(e_g)^2$, green $(2p_{1/2})^2(2p_{3/2})^3(t_{2g})^5(e_g)^3$, blue $(2p_{1/2})^2(2p_{3/2})^3(t_{2g})^4(e_g)^4$, magenta $(2p_{1/2})^1(2p_{3/2})^4(t_{2g})^6(e_g)^2$, yellowish green $(2p_{1/2})^1(2p_{3/2})^4(t_{2g})^5(e_g)^3$, and cyan $(2p_{1/2})^1(2p_{3/2})^4(t_{2g})^4(e_g)^4$. (b) Compositions of final configurations for the dipole-allowed transitions.

representations were obtained by the present multielectron calculation. They are distinguished according to their final configurations, as shown in Fig. 4(a). Similar to the other two systems, some mixtures among different configurations can be seen as the overlapping of colored areas. The contributions from the six final configurations are shown in Fig. 4(b). Despite the presence of many final states, theoretical Ni $L_{2,3}$ NEXAFS looks simple when the initial state is low spin. It is composed of two strong peaks, *b* and *e*, with tiny satellite peaks. This is because only $(2p_{1/2})^2(2p_{3/2})^3(t_{2g})^6(e_g)^1$ [red bars in Fig. 4(a)] and $(2p_{1/2})^1(2p_{3/2})^4(t_{2g})^6(e_g)^1$ configurations [magenta bars in Fig. 4(a)] are allowed as an electric dipole transition. On the other hand, two other calculations with different initial states produce completely different theoretical NEXAFS. (Theoretical NEXAFS from the middle-spin state is not shown in Fig. 4.) This clearly implies that the $L_{2,3}$ NEXAFS can be used to identify initial electronic states of Ni if reliable theoretical spectra or referential spectra are available.

4. Comparison to experimental spectra

In order to examine the adequacy of theoretical results obtained in the present study, we conducted ELNES experi-

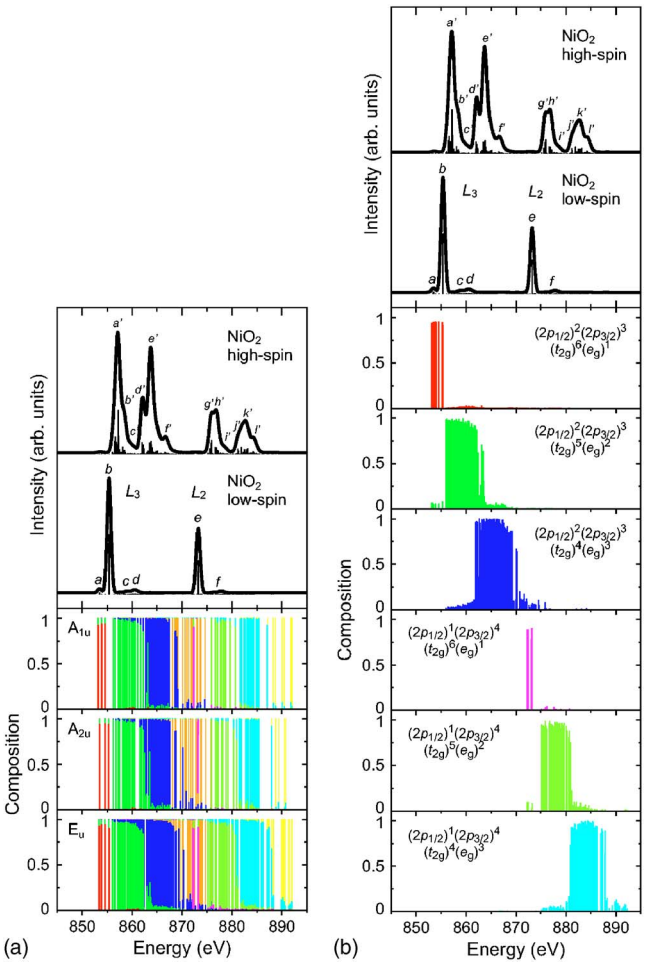

FIG. 4. (Color online) (a) Theoretical $L_{2,3}$-edge NEXAFS and ELNES for low and high-spin states for Ni(IV) in NiO_2 are shown in upper two panels. The following panels show the composition of final configurations for multielectron eigenstates in A_{1u}, A_{2u}, and E_u symmetries. They are classified according to final configurations as distinguished by colors: red $(2p_{1/2})^2(2p_{3/2})^3(t_{2g})^6(e_g)^1$, green $(2p_{1/2})^2(2p_{3/2})^3(t_{2g})^5(e_g)^2$, blue $(2p_{1/2})^2(2p_{3/2})^3(t_{2g})^4(e_g)^3$, orange $(2p_{1/2})^2(2p_{3/2})^3(t_{2g})^3(e_g)^4$, magenta $(2p_{1/2})^1(2p_{3/2})^4(t_{2g})^6(e_g)^1$, yellowish green $(2p_{1/2})^1(2p_{3/2})^4(t_{2g})^5(e_g)^2$, cyan $(2p_{1/2})^1(2p_{3/2})^4(t_{2g})^4(e_g)^3$, and yellow $(2p_{1/2})^1(2p_{3/2})^4(t_{2g})^3(e_g)^4$. (b) Compositions of final configurations for the dipole-allowed transitions.

ments using transmission electron microscopy. Samples were commercial NiO powder, $LiNiO_2$ prepared by a solid-state method,[12] and a NiO_2 sample obtained by electrochemical lithium extraction from $LiNiO_2$. ELNES was measured with energy resolution ranging from 0.8 to 1.0 eV FWHM of a zero-loss peak. More detail of the experimental procedure can be found elsewhere.[20]

Figure 5 shows the experimental Ni $L_{2,3}$ ELNES of (a) NiO, (b) $LiNiO_2$, and (c) NiO_2. The experimental Ni $L_{2,3}$ NEXAFS of NiO with higher energy resolution is also shown below the ELNES for comparison. This spectrum was measured at BL25SU at SPring-8 (Hyogo, Japan), using the same sample as the ELNES measurement. As can be seen, not only the peak positions but also the spectral shapes of these three compounds are discernibly different. This clearly

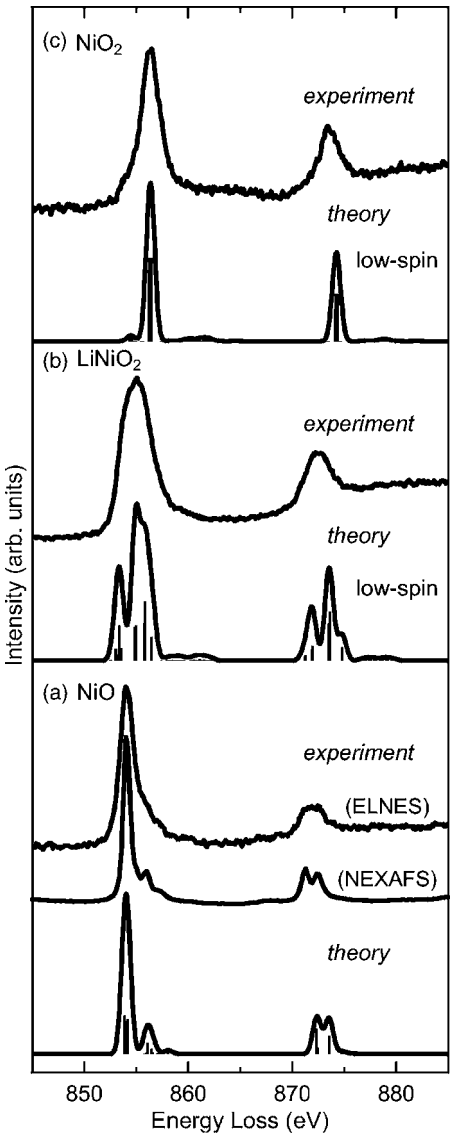

FIG. 5. Experimental Ni $L_{2,3}$-edge ELNES of (a) NiO, (b) $LiNiO_2$, and (c) NiO_2 as compared to theoretical spectra. For NiO, Ni $L_{2,3}$ NEXAFS with a higher energy resolution is also shown to see detailed structures. For theoretical spectra of $LiNiO_2$ and NiO_2, low-spin states are chosen as initial states. The absolute transition energy of the theoretical spectrum of NiO, $LiNiO_2$, and NiO_2 are shifted by 1.9, 1.6, and 1.2 eV, respectively, in order to see best matches with experimental spectra.

implies that electronic structures of Ni in the three compounds are quite different. Theoretical spectra of the three compounds showing best agreement to experimental spectra are displayed below the corresponding experimental spectra in Fig. 5. The energy scales of the theoretical spectra are translated in order to see the best matches with experimental spectra. Because the magnitude of chemical shift from NiO to NiO_2 is slightly overestimated, the magnitudes of translations are 1.9, 1.6, and 1.2 eV, for NiO, $LiNiO_2$ and NiO_2, respectively. In these theoretical spectra, low-spin states are chosen for $LiNiO_2$ and NiO_2 as initial states. Spectral shape of these two compounds cannot be explained with the other initial states. We can therefore conclude that the ground state of Ni atoms is Ni(II) in NiO as widely accepted, Ni(III) with low-spin state in $LiNiO_2$, and Ni(IV) with low-spin state in NiO_2. A remaining problem is a small overestimation of the chemical shift from NiO to NiO_2 by 0.7 eV. This may be ascribed to the use of small clusters in the present calculations, which needs to be clarified in the future. Currently, larger calculations are prohibitively expensive.

Ni $L_{2,3}$ NEXAFS of NiO and $LiNiO_2$ was reported by Montoro *et al.* in 1999.[21] They found that the NEXAFS of $LiNiO_2$ was similar to that of NiO and concluded that the Ni ions in both of $LiNiO_2$ and NiO were Ni(II). In the present work, ELNES of $LiNiO_2$ is clearly different from that of NiO. The origin of the discrepancy has been discussed in Ref. 20. The spectra reported in Ref. 21 may reflect the electronic structure at the surface of the sample, but not the bulk.

IV. SUMMARY AND CONCLUSIONS

First-principles multielectron calculations of Ni $L_{2,3}$ NEXAFS and ELNES of NiO, $LiNiO_2$, and NiO_2 have been made. Theoretical spectra not only satisfactorily reproduce the experimental spectra, but can also be used to interpret the experimental spectra. The present method is based on the robust multielectron quantum theory, which could be applied to the analysis and prediction of $L_{2,3}$-edge spectra of other transition-metal compounds. The major parts of the present study can be summarized as follows:

1. Relativistic four-component wave functions of molecular orbitals were obtained by solving Dirac equations within the local density approximation using model clusters of NiO_6^{m-}, where m is taken to be 10, 9, and 8 for NiO, $LiNiO_2$, and NiO_2, respectively.

2. Slater determinants composed of all Ni-2p and 3d orbitals in NiO_6^{m-} clusters were constructed using the relativistic molecular orbitals. Multielectron wave functions expressed by a linear combination of the Slater determinants were obtained by diagonalizing the multielectron Hamiltonian. The number of Slater determinants for the initial states was 45, 120, and 210 for NiO, $LiNiO_2$, and NiO_2, respectively. It was, respectively, 60, 270, and 720 for the final states. The eigenstates were analyzed in terms of symmetry and composition of electronic configurations.

3. The contributions of O-2p orbitals through covalency can be automatically included without any other scheme, since the multielectron calculations were made using molecular orbitals instead of atomic orbitals. This is very important for transition-metal oxides with high formal charges, such as Ni(III) and Ni(IV).

4. Theoretical NEXAFS and ELNES within the electric dipole approximation were obtained by calculating oscillator strengths from several initial states to all of final states. Differences because of the initial states were discussed. The origin of satellite peaks in these spectra was also discussed.

5. Experimental ELNES for the three compounds were satisfactorily reproduced by the present calculations, which unambiguously show that Ni atoms are Ni(III) with a low-spin state in $LiNiO_2$, and Ni(IV) with a low-spin state in NiO_2.

ACKNOWLEDGMENTS

This work was supported by three programs from Ministry of Education, Science, Sports, and Culture of Japan, i.e., (i) Grant-in-aid for Scientific Research on Priority Areas (No. 751), (ii) Computational materials science unit in Kyoto University, and (iii) twenty-first century COE program. H.I., Y.K., and T. M. thank the Japan Society for the Promotion of Science (JSPS) for their research fellowship. NEXAFS measurement at SPring-8 was made under Proposal No. 2004A0402-NSc-np-Na.

[1] J. J. Rehr and R. C. Albers, Rev. Mod. Phys. **72**, 621 (2000).
[2] A. Filipponi, A. Di Cicco, and C. R. Natoli, Phys. Rev. B **52**, 15122 (1995).
[3] A. Filipponi and A. Di Cicco, Phys. Rev. B **52**, 15135 (1995).
[4] S.-D. Mo and W. Y. Ching, Phys. Rev. B **62**, 7901 (2000).
[5] T. Mizoguchi, I. Tanaka, S. Yoshioka, M. Kunisu, T. Yamamoto, and W. Y. Ching, Phys. Rev. B **70**, 045103 (2004).
[6] T. Yamamoto, T. Mizoguchi, and I. Tanaka, Phys. Rev. B **71**, 245113 (2005).
[7] A. L. Ankudinov, A. I. Nesvizhskii, and J. J. Rehr, Phys. Rev. B **67**, 115120 (2003).
[8] P. Kruger and C. R. Natoli, Phys. Rev. B **70**, 245120 (2004).
[9] F. M. F. de Groot, J. Electron Spectrosc. Relat. Phenom. **67**, 529 (1994).
[10] F. de Groot, Chem. Rev. (Washington, D.C.) **101**, 1779 (2001).
[11] K. Ogasawara, T. Iwata, Y. Koyama, T. Ishii, I. Tanaka, and H. Adachi, Phys. Rev. B **64**, 115413 (2001).
[12] T. Ohzuku, A. Ueda, and M. Nagayama, J. Electrochem. Soc. **140**, 1862 (1993).
[13] C. A. Barrett and E. B. Evans, J. Am. Ceram. Soc. **47**, 533 (1964).
[14] A. Rosen, D. E. Ellis, H. Adachi, and F. W. Averill, J. Chem. Phys. **65**, 3629 (1976).
[15] T. Ishii, K. Ogasawara, H. Adachi, and I. Tanaka, J. Chem. Phys. **115**, 492 (2001).
[16] T. Ishii, M. G. Brik, and K. Ogasawara, J. Alloys Compd. **380**, 136 (2004).
[17] S. Watanabe and H. Kamimura, Mater. Sci. Eng., B **3**, 313 (1989).
[18] R. S. Mulliken, J. Chem. Phys. **23**, 1833 (1955).
[19] F. A. Cotton, *Chemical Applications of Group Theory* (Wiley, New York, 1990).
[20] Y. Koyama, T. Mizoguchi, H. Ikeno, and I. Tanaka, J. Phys. Chem. B **109**, 10749 (2005).
[21] L. A. Montoro, M. Abbate, E. C. Almeida, and J. M. Rosolen, Chem. Phys. Lett. **309**, 14 (1999).